Abdominal Radiology (2020) 45:332–341
https://doi.org/10.1007/s00261-019-02272-0

PELVIS

The usefulness of *b* value threshold map in the evaluation of rectal adenocarcinoma

Fu Shen[1] · Luguang Chen[1] · Zhihui Li[1] · Haidi Lu[1] · Yukun Chen[1] · Zhen Wang[1] · Caixia Fu[2] · Robert Grimm[3] · Jianping Lu[1]

Published online: 23 October 2019

Abstract

Purpose To investigate the usefulness of *b* value threshold ($b_{Threshold}$) map in the evaluation of rectal adenocarcinoma by comparing it with diffusion-weighted images and ADC maps regarding lesion detection and the prediction of pathological features.

Materials and Methods Thirty-five patients with rectal tumors were enrolled and underwent axial DWI using a 3-Tesla MRI system. Contrast-to-noise ratio (CNR) between the lesions and normal tissues were assessed on the diffusion-weighted images and $b_{Threshold}$ maps. Reproducibility for ADC and $b_{Threshold}$ values were assessed. Significant differences between different groups for pathological prognostic factors were evaluated. Diagnostic performance of ADC and $b_{Threshold}$ values for those factors were assessed.

Results Reproducibility was excellent for the ADC and $b_{Threshold}$ values (ICC 0.985 and 0.992; CV 3.8% and 4.0%) measurements. The CNR between lesions and normal tissues on $b_{Threshold}$ maps was significantly higher than that on diffusion-weighted images (9.91 ± 5.35 vs. 7.68 ± 3.08, $p = 0.012$). There were significant differences in the ADC and $b_{Threshold}$ values between different pathologic differentiation degrees and T stages; significant difference was observed in the $b_{Threshold}$ values between the different N stage groups (all p values < 0.050). No significant differences were observed between the ROC curves of ADC and the $b_{Threshold}$ values of rectal lesions for pathologic differentiation and T stage. $b_{Threshold}$ maps showed good diagnostic performance for N stage.

Conclusion Both ADC and $b_{Threshold}$ values can differentiate between degrees of pathologic differentiation and T1-2 versus T3-4. Potential added advantages however of the $b_{Threshold}$ map include a higher CNR compared with DWI images, thereby improving lesion visualization detection, and better diagnostic performance for end staging than ADC. Thus, the $b_{Threshold}$ map may compliment DWI and ADC to evaluate pathologic features of rectal primary tumors and metastatic lymph nodes.

Keywords Rectum · Adenocarcinoma · Diffusion magnetic resonance imaging · Pathology

Introduction

Colorectal cancer (CRC) has the third highest incidence among malignant tumors worldwide [1]. According to the most recent data reported by the Cancer Incidence and Mortality of China, CRC ranks fifth cancer in incidence and mortality in both men and women [2]. Among all CRC patients, rectal cancer accounts for 30–35% of these cases. Determining an optimal treatment plan is a complex process for patients with rectal cancer because it often consists of a combination of surgery, chemotherapy, and radiation therapy [3, 4]. For example, surgery is the standard treatment strategy for early rectal cancer (T1-2, and N0), and neoadjuvant chemoradiotherapy followed by total mesorectal excision

Fu Shen and Luguang Chen contributed equally to this work.

✉ Jianping Lu
cjr.lujianping@vip.163.com

[1] Department of Radiology, Changhai Hospital of Shanghai, Second Military Medical University, No. 168 Changhai Road, Shanghai 200433, China

[2] MR Application Development, Siemens Shenzhen Magnetic Resonance Ltd, Shenzhen, China

[3] MR Applications Pre-development, Siemens Healthcare, Erlangen, Germany

(TME) is the treatment for locally advanced (T3-4 and/or N1-2) rectal cancer [3]. Appropriate treatment decisions depend on accurate preoperative staging, which is based on the pathological type, degree of differentiation, depth of tumor infiltration, and the presence or absence of regional lymph node (LN) metastasis, factors that can predict the invasiveness and prognosis of a tumor [3]. Therefore, an in-depth understanding of the pathological features of a tumor is particularly important in predicting prognosis and formulating a clinical treatment plan.

Diffusion-weighted imaging (DWI) is a non-invasive technique to evaluate the microscopic mobility of water molecules in organs or lesions without using an exogenous contrast agent. It has been used clinically to detect and evaluate rectal tumors [5–7]. The DWI-derived apparent diffusion coefficient (ADC), indicating the diffusivity of water, can reflect the histological characteristics of lesions and has also been employed in the diagnosis of rectal cancer and evaluation of its response to treatment [8, 9]. Single-shot echo-planar imaging (SS EPI) with a mono-exponential model is the most commonly used DWI technique to evaluate rectal cancer due to its fast acquisition time and decreased vulnerability to motion artifacts. High *b* values (1000–2000 s/mm^2) improve the lesion visualization in rectal cancer [10, 11]. However, high *b* values make SS EPI images more vulnerable to image distortion, prolong the scan time and cause a low signal-to-noise ratio [12]. To balance the image quality with lesion visualization, diffusion-weighted images at *b* values ranging from 0 to 1000 s/mm^2 are commonly used [6, 13–18]. The diffusion-weighted images are used for visual screening of the lesions due to their positive contrast, while ADC maps with their negative contrast serve as supplementary images for diagnosis and are also used to determine T2 effects [19]. Nevertheless, the image contrast for lesion screening is not always satisfactory.

Recently, a novel diffusion contrast method, the *b* value threshold ($b_{\text{Threshold}}$) map, was proposed [19]. The intensity of a $b_{\text{Threshold}}$ map indicates the *b* value at which the diffusion signal decreases below a given threshold in a signal model (e.g., mono-exponential model for ADC calculation). $b_{\text{Threshold}}$ maps have a positive contrast and are similar to diffusion-weighted images regarding lesion detection [19]. Specifically, compared with normal tissues, rectal tumors showed hyperintensity in $b_{\text{Threshold}}$ maps, while the lesions displayed hypointensity in ADC maps. It has been demonstrated that $b_{\text{Threshold}}$ maps can potentially provide better lesion visualization for the prostate than acquired or computed high *b* value diffusion-weighted images or ADC maps [19]. However, the evaluation of rectal lesions using $b_{\text{Threshold}}$ maps has not been explored so far.

Therefore, the purpose of the present study was to investigate the value of $b_{\text{Threshold}}$ maps in the evaluation of rectal adenocarcinoma by comparing it with high *b* value diffusion-weighted images and ADC maps regarding lesion detection and prediction of pathological features.

Materials and methods

Subjects

This retrospective study was approved by the local institutional review board, and the need to obtain informed consent was waived. Between March 2018 and September 2018, 45 consecutive treatment-naive patients with rectal lesions identified by colonoscopy were enrolled in the study. The exclusion criteria were as follows: (1) received chemotherapy or radiotherapy before or/and after MRI ($n=3$), (2) contraindications to magnetic resonance imaging ($n=1$), (3) poor image quality ($n=2$), (4) with distant metastases ($n=0$), and (5) lesions confirmed as mucinous adenocarcinoma ($n=4$). Rectal mucinous adenocarcinomas were excluded because they were more aggressive than adenocarcinomas, and their behavior is distinctive on T2WI and DWI images. All the patients underwent rectal MRI and surgery. Postoperative blood draw samples were collected so that carcinoembryonic antigen (CEA) and carbohydrate antigen 19-9 (CA19-9) values could be obtained for each patient. A value of CEA < 5 ng/ml was defined as negative, and a value of CA19-9 < 37 U/ml was defined as negative. Therefore, 35 patients with rectal adenocarcinoma were included in the final analysis.

Magnetic resonance imaging

All MRI examinations were performed using a 3-Tesla MRI scanner (MAGNETOM Skyra, Siemens Healthcare, Erlangen, Germany), an 18-channel phased-array body coil and an integrated spine coil. As demonstrated in a previous study, the optimal *b* value combination of 0 and 1000 s/mm^2 was recommended for DWI of the rectum [20]. Therefore, axial SS EPI DWI with those 2 *b* values was used and the main scanning parameters were as follows: repetition time/echo time (TR/TE): 6300/89 ms; field of view (FOV): 380 × 380 mm^2; matrix: 150 × 150; number of slices: 20; slice thickness: 5 mm; gap: 1 mm; acceleration factor: 2; bandwidth: 2084 Hz/pixel; *b* values (number of averages): 0 (1) and 1000 (3) s/mm^2; diffusion directions were applied in three orthogonal directions; and acquisition time: 1 min 30 s. Transversal high-resolution T2-weighted turbo spin echo images were acquired using the following parameters: TR/TE: 4000/108 ms; FOV: 180 × 180 mm^2; matrix: 320 × 320; slice thickness: 3 mm; gap: 0 mm; acceleration factor: 3; echo train length: 16; and acquisition time: 4 min 10 s.

Image analysis

All DW images were sent to a dedicated workstation and were independently assessed by two experienced observers (ZL and FS, with 6 and 8 years of experience in radiology, respectively) using a prototype post-processing tool (Body Diffusion Toolbox, Siemens Healthcare, Germany). ADC maps were calculated from DW images with two b values using the mono-exponential model $S(b) = S_0 * e^{-b*ADC}$, where S_0 and $S(b)$ represents the signal intensity without ($b = 0$ s/mm^2) and with ($b > 0$ s/mm^2) diffusion weighting, respectively, while the following formula was used to derive the $b_{\text{Threshold}}$ maps: $b_{\text{Threshold}} = -1/ADC * log(Threshold/S_0)$, with *Threshold* defined as 50 (a.u.) for rectal applications. The intensities of b value map indicate the b value at which the diffusion signal drops under a given threshold.

The regions of interest (ROIs), for the single slice with the maximum tumor size, were manually outlined by the two observers on rectal lesions on ADC and $b_{\text{Threshold}}$ maps. The ROI-based mean values of the ADC and $b_{\text{Threshold}}$ and areas of ROIs were recorded. The contrast-to-noise ratios (CNRs) of the diffusion-weighted images with $b = 1000$ s/mm^2 and $b_{\text{Threshold}}$ maps were determined as $CNR = |SI_{\text{lesion}} - SI_{\text{gluteus maximus}}|/(\sigma^2_{lesion} + \sigma^2_{\text{gluteus maximus}})^{1/2}$, where SI and σ refer respectively to the mean signal intensity and standard deviation of the ROI of the specified tissue, such as the lesion or gluteus maximus.

Pathological evaluation

The tissue sections underwent hematoxylin-eosin staining. All lymph nodes from the mesorectal surgical specimens were extracted to ensure that at least 12 lymph nodes per patient were collected. The final histopathology reports contained the tumor TN staging, histological grade, presence of perineural invasion, presence of lymph-vascular invasion (LVI), tumor deposits, and descriptions of the circumferential resection margins (CRM) [21]. All TN statuses were determined according to the American Joint Committee on Cancer staging system, 7th edition [22]. Regarding pathological features, patients were divided into two groups according to the following categories: histological grade: high-moderate and poor differentiation; T stage: T1-2 and T3-4 stages; and N stage: N0 and N1-2 stages. Regarding other clinical features, such as perineural invasion, lymph-vascular invasion, tumor deposits, CRM, CEA, and CA19-9, the patients were divided into two groups according to the presence of negative or positive results.

Statistical analysis

SPSS software (version 16.0, Inc., Chicago, IL, USA) and MedCalc (version 13.0.0.0, MedCalc Softaware, Mariakerke, Belgium) were used for statistical analyses. Continuous variables are presented as the mean ± standard deviation, and categorical variables are expressed as percentages. The Kolmogorov-Smirnov test was used to assess the normal distribution of data. Interobserver reproducibility for the ADC and $b_{\text{Threshold}}$ values was assessed using intraclass coefficients (ICCs), coefficients of variability (CVs), and Bland-Altman plots. ICC values > 0.75 indicated excellent agreement, 0.4 to 0.75 indicated good agreement, and < 0.4 indicated poor agreement [23]. Significant differences in the CNR between diffusion-weighted images with b value = 1000 s/mm^2 and $b_{\text{Threshold}}$ maps were assessed using paired-sample t tests. Significant differences in ADC and $b_{\text{Threshold}}$ values between different groups for pathological prognostic factors were evaluated using independent sample t tests. Areas of ROIs between ADC and $b_{\text{Threshold}}$ maps were compared using paired-sample t tests. For the statistically significant prognostic factors, the diagnostic performance of the ADC and $b_{\text{Threshold}}$ values for those factors were assessed using receiver operating characteristic (ROC) curves. Significant differences in the ADC and $b_{\text{Threshold}}$ values between areas under the curve (AUCs) were assessed using the comparison of ROC curves. A p value < 0.05 was inferred to indicate statistical significance.

Results

Patient demographics

Thirty-five patients with rectal adenocarcinomas were included in the final analysis. There were 27 males and 8 females, with a mean age of 55.7 ± 9.2 years (range 36–74 years). Total mesorectal excision occurred at a time interval of 8.9 ± 5.8 (range 3–22) days after imaging. The numbers of tumors located in the superior, middle, and lower rectum were 11, 14, and 10, respectively. Regarding the degree of pathological differentiation, there were 2 patients with high differentiation, 27 patients with moderate differentiation, and 6 patients with poor differentiation. For the T stage, there were 4, 10, 19, and 2 patients of T1, T2, T3, and T4, respectively. Regarding the N stage, 14 (40.0%) patients had regional lymph node metastases, while 21 (60.0%) patients had no lymph node metastases. There were 11 (31.4%), 12 (34.3%), 13 (37.1%), 11 (31.4%), and 4 (11.4%) patients showing positive tumor deposits, positive perineural invasion, positive

Table 1 Patient demographics

Variable	$n = 35$ (%)
Gender	
Male	27 (77.1)
Female	8 (22.9)
Age (years)	
Mean ± SD	55.7 ± 9.2
Location	
Upper	11 (31.4)
Middle	14 (40.0)
Lower	10 (28.6)
Pathological differentiation	
High	2 (5.7)
Moderate	27 (77.1)
Poor	6 (17.1)
T stage	
T1	4 (11.4)
T2	10 (28.6)
T3	19 (54.3)
T4	2 (5.7)
N stage	
N0	21 (60.0)
N1	6 (17.1)
N2	8 (22.9)
Tumor deposits	
Negative	24 (68.6)
Positive	11 (31.4)
Perineural invasion	
Negative	23 (65.7)
Positive	12 (34.3)
Lymph-vascular invasion	
Negative	22 (62.9)
Positive	13 (37.1)
CEA	
Negative	24 (68.6)
Positive	11 (31.4)
CA19-9	
Negative	31 (88.6)
Positive	4 (11.4)

CA19-9 carbohydrate antigen 19-9, *CEA* carcinoembryonic antigen, *SD* standard deviation

lymph-vascular invasion, positive CEA, and positive CA19-9, respectively (Table 1). None had positive CRM.

Interobserver variability of ADC and $b_{Threshold}$

The statistical results of the interobserver variability of the ADC and $b_{Threshold}$ measurements are presented in Table 2. There was excellent reproducibility for those measurements, with ICC and CV values of 0.985 (0.970–0.992) and 3.8% for ADC measurements, and 0.992 (0.984–0.996) and 4.0% for $b_{Threshold}$ measurements, respectively. Additionally, the bias and limit of agreement were relatively low for those measurements: 0.013 (−0.110 to 0.083) and 0.044 (−0.129 to 0.216) for ADC and $b_{Threshold}$ measurements using Bland-Altman plots, respectively (Fig. 1).

CNR and ROI size

A significant difference was observed in the CNR between diffusion-weighted images with b value = 1000 s/mm^2 and $b_{Threshold}$ maps (7.68 ± 3.08 vs. 9.91 ± 5.35, $p = 0.012$). There was no significant difference between the two observers in outlining the ROI size (345.4 ± 178.1 mm^2 vs. 341.8 ± 166.7 mm^2, $p = 0.845$).

ADC and $b_{Threshold}$ in relation to different prognostic factors

Table 3 summarizes the statistical analyses evaluating the relationships among ADC, $b_{Threshold}$ and different pathological prognostic factors. Significant differences in ADC (0.984 ± 0.192 vs. 0.747 ± 0.108 × 10^{-3} mm^2/s, $p = 0.006$) and the $b_{Threshold}$ (1.643 ± 0.493 vs. 2.139 ± 0.231 × 10^3 s/mm^2, $p = 0.023$) were found between high/moderate and poor pathologic differentiation histological grades, respectively. There were significant differences observed between T1-2 and T3-4 patients in the ADC (1.106 ± 0.162 vs. 0.835 ± 0.142 × 10^{-3} mm^2/s, $p < 0.001$) and $b_{Threshold}$ (1.431 ± 0.443 vs. 1.927 ± 0.429 × 10^3 s/mm^2, $p = 0.002$) measurements, respectively. The $b_{Threshold}$ value was significantly larger in patients with N1-2 than in those with N0 (1.978 ± 0.344 vs. 1.562 ± 0.515 × 10^3 s/mm^2, $p = 0.012$), while no significant difference in ADC was found between these 2

Table 2 Interobserver variability of ADC and $b_{Threshold}$ measurements

Parameters	Observers	Mean ± SD	ICC (95% CI)	Bias (LoA)	CV (%)
ADC[a]	# 1	0.937 ± 0.191	0.985 (0.970–0.992)	0.013 (−0.110 to 0.083)	3.8
	# 2	0.950 ± 0.213			
$b^b_{Threshold}$	# 1	1.750 ± 0.502	0.992 (0.984–0.996)	0.044 (−0.129 to 0.216)	4.0
	# 2	1.707 ± 0.490			

CV coefficient of variability, *ICC* intraclass coefficient, *LoA* limit of agreement, *SD* standard deviation

[a] × 10^{-3} mm^2/s

[b] × 10^3 s/mm^2

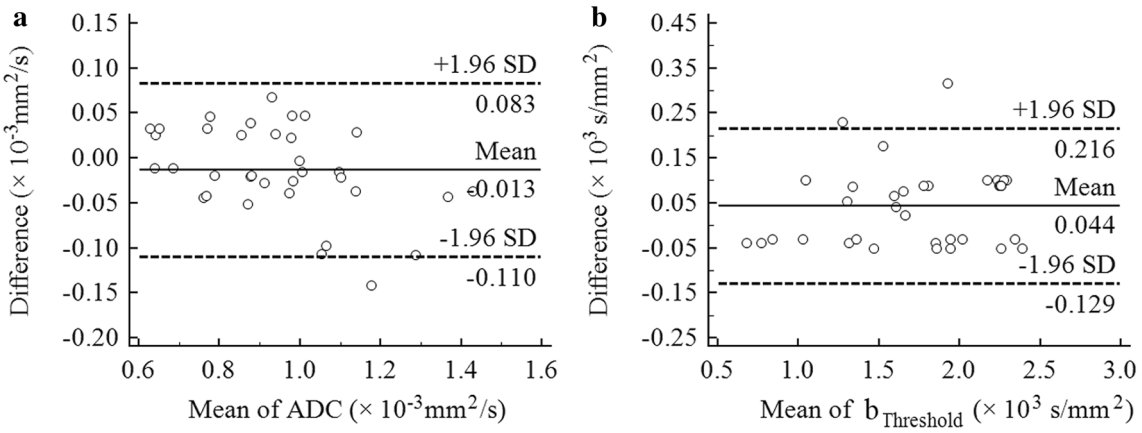

Fig. 1 Bland-Altman plots showing the interobserver reproducibility of ADC (**a**) and $b_{Threshold}$ (**b**) measurements

Table 3 The differences in ADC and $b_{Threshold}$ values between different groups for pathological prognostic factors

Prognostic factors	Groups	Patients (*n*)	ADC (mean ± SD, × 10^{-3} mm^2/s)	*p* value	$b_{Threshold}$ (mean ± SD, × 10^3 s/mm^2)	*p* value
Pathologic differentiation	High/moderate	29	0.984 ± 0.192	*0.006*	1.643 ± 0.493	*0.023*
	Poor	6	0.747 ± 0.108		2.139 ± 0.231	
T stage	T1-2	14	1.106 ± 0.162	*< 0.001*	1.431 ± 0.443	*0.002*
	T3-4	21	0.835 ± 0.142		1.927 ± 0.429	
N stage	N0	21	0.997 ± 0.211	0.050	1.562 ± 0.515	*0.012*
	N1-2	14	0.862 ± 0.158		1.978 ± 0.344	
Tumor deposits	Negative	24	0.926 ± 0.197	0.455	1.744 ± 0.512	0.785
	Positive	11	0.981 ± 0.211		1.694 ± 0.474	
Perineural invasion	Negative	23	0.926 ± 0.203	0.497	1.726 ± 0.499	0.972
	Positive	12	0.976 ± 0.200		1.733 ± 0.506	
Lymph-vascular invasion	Negative	22	0.955 ± 0.221	0.489	1.719 ± 0.467	0.864
	Positive	13	0.942 ± 0.187		1.776 ± 0.531	
CEA	Negative	24	0.966 ± 0.199	0.388	1.682 ± 0.465	0.424
	Positive	11	0.895 ± 0.203		1.829 ± 0.562	
CA19-9	Negative	31	0.962 ± 0.192	0.135	1.682 ± 0.482	0.127
	Positive	4	0.802 ± 0.233		2.085 ± 0.502	

p value < 0.05 are given in italics

ADC apparent diffusion coefficient, *CA19-9* carbohydrate antigen 19-9, *CEA* carcinoembryonic antigen, *SD* standard deviation

groups. No significant difference in the ADC or $b_{Threshold}$ values was found between the different groups for tumor deposits, perineural invasion, lymph-vascular invasion, CEA, and CA19-9 (all $p > 0.050$). Representative images from rectal carcinoma patients with T1N0, T2N0, and T3N2 stages are shown in Figs. 2 and 3.

Diagnostic performance of ADC and $b_{Threshold}$

The results of the ROC analyses are displayed in Table 4. Figure 4 shows the receiver operating characteristic (ROC) curves of ADC and $b_{Threshold}$ for the statistically significant prognostic factors. For pathologic differentiation, the AUC, sensitivity, and specificity were 0.868, 100.0%, and 69.0% for the ADC and 0.810, 100.0%, and 55.2% for the $b_{Threshold}$ values, respectively. For T stage, the AUC, sensitivity, and specificity were 0.912, 90.5%, and 85.7% for the ADC and 0.796, 52.4%, and 100.0% for the $b_{Threshold}$ values, respectively. When using $b_{Threshold}$ for N stage, the AUC, sensitivity, and specificity were 0.735, 85.70%, and 66.70%, respectively. No significant differences were found between the

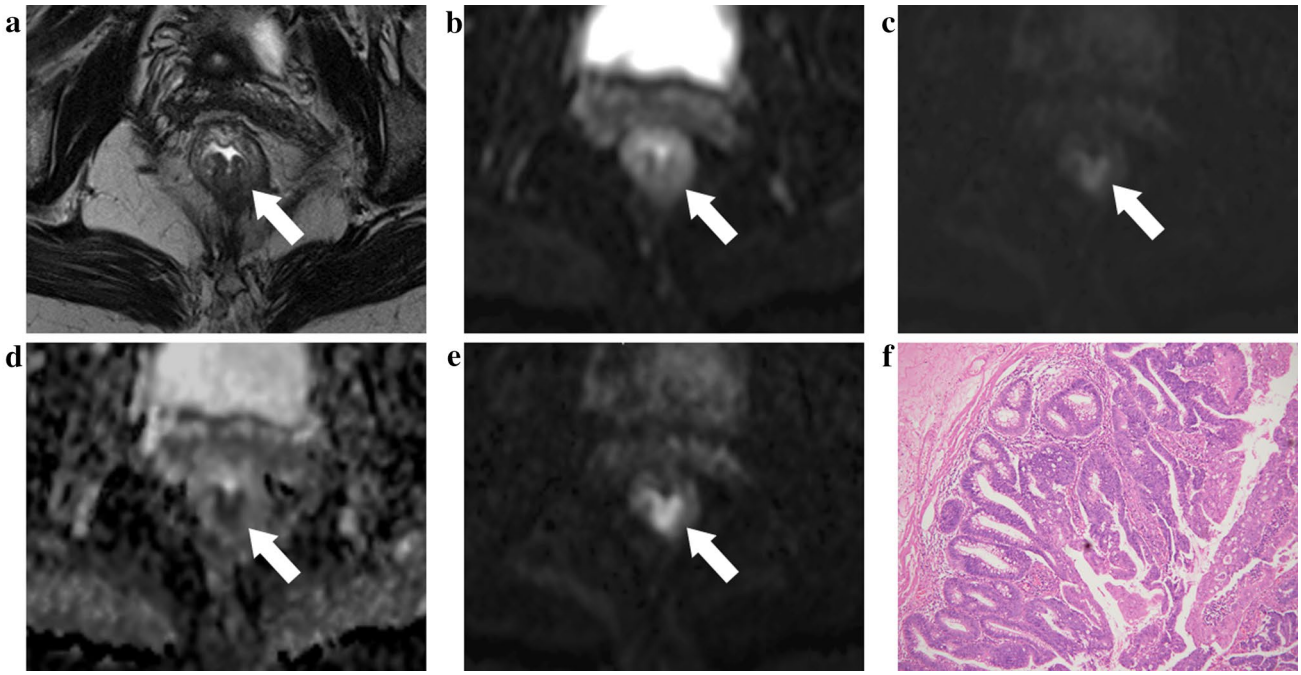

Fig. 2 All images were from a 58-year-old man with moderately differentiated adenocarcinoma. (**a**) Axial T2 W image shows abnormal signals on the posterior side of the rectal wall (Arrow). (**b**) Axial image with $b=0$ s/mm^2 shows abnormal signals on the posterior side of the rectal wall (Arrow). (**c**) DWI with $b=1000$ s/mm^2 shows the lesion with hyperintensity (Arrow). (**d**) The ADC map shows the lesion with hypointensity (Arrow), ADC$=1.146\times10^{-3}$ mm^2/s. (**e**) The b value threshold map shows the lesion with hyperintensity (Arrow), $b_{\text{Threshold}}=1.223\times10^{3}$ s/mm^2, and the CNR values were 2.2 and 6.9 for the DWI image with $b=1000$ s/mm^2 and $b_{\text{Threshold}}$, respectively. (**f**) Postoperative pathology results (hematoxylin and eosin, ×100). Tumor cells invaded the muscularis propria layer but did not extend beyond, confirming staging as T2N0

ADC and $b_{\text{Threshold}}$ in the AUC for pathologic differentiation (0.057, $p=0.363$) and T stage (0.116, $p=0.092$).

Discussion

Optimal treatment for rectal cancer depends on accurate diagnosis and staging. In the present study, we investigated the value of $b_{\text{Threshold}}$ maps generated from DWI images in the evaluation and staging of rectal cancer. The reproducibility of $b_{\text{Threshold}}$ values was excellent with an ICC of 0.992, CV of 4.0% and narrow intervals observed on Bland-Altman plots, suggesting that interobserver variability will be low if used clinically.

In the present study, a new $b_{\text{Threshold}}$ map, derived from diffusion-weighted images, in which intensities indicate the b value at which the diffusion signal drops under a predefined value. Unlike to ADC maps, $b_{\text{Threshold}}$ maps are visually more appropriate to the doctor's reading habits and are similar to diffusion-weighted images in which the tumors showed hyperintensity compared with normal tissues. Our results showed that $b_{\text{Threshold}}$ maps offered significantly higher CNR than DWI images with a b value $=1000$ s/mm^2, suggesting that $b_{\text{Threshold}}$ maps can significantly improve the signal contrast between lesions and normal tissue. Such signal contrast is useful for detecting rectal lesions, which are highly heterogeneous, irregularly shaped, and often cannot be easily distinguished from the surrounding adipose tissues due to inflammation and blood vessel invasion [17]. Improved conspicuity would also allow for more accurately drawn ROIs for quantitative measurements.

The present study also demonstrated that the $b_{\text{Threshold}}$ values were higher in poorly differentiated tumors than in highly/moderately differentiated tumors and that the ADC values were lower in poorly differentiated tumors than in highly/moderately differentiated tumors. The latter finding is consistent with previous studies [24–26]. The ability of the $b_{\text{Threshold}}$ values to distinguish between differentiation types is clinically helpful because determining differentiation may contribute to selecting an appropriate treatment plan.

The ADC value of group T3-4 was significantly lower than that in group T1-2, and the $b_{\text{Threshold}}$ value of group T3-4 was higher than that in group T1-2. These findings could be explained by tumors with higher T stage showing greater heterogeneity of cell morphology and histology, higher cell density, and smaller interstitia. Furthermore, all the ROC curves showed large AUCs (>0.7), suggesting

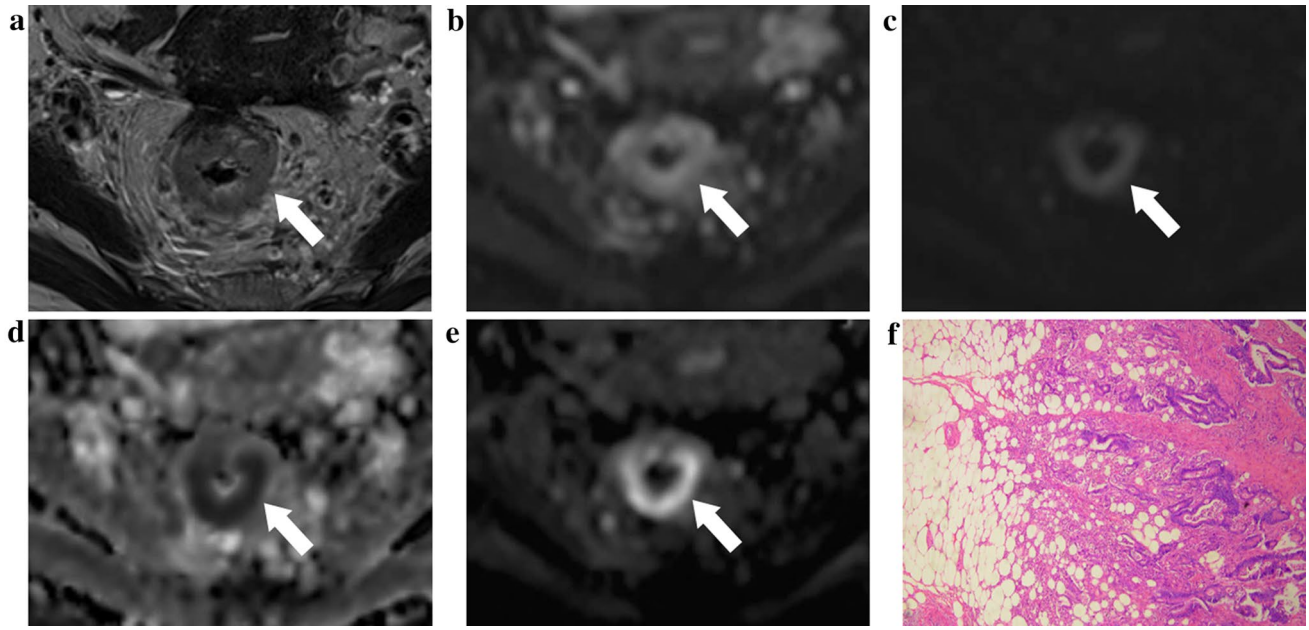

Fig. 3 All the images were from a 61-year-old woman with poorly differentiated adenocarcinoma. (**a**) Axial T2 W image shows circular abnormal signals in the rectal wall (Arrow). (**b**) Axial image with $b=0$ s/mm^2 shows circular abnormal signals in the rectal wall (Arrow). (**c**) DWI image with $b=1000$ s/mm^2 shows the lesion with hyperintensity (Arrow). (**d**) The ADC map shows the lesion with hypointensity (Arrow), ADC$=0.788\times10^{-3}$ mm^2/s. (**e**) The b value threshold map shows the lesion with hyperintensity (Arrow), $b_{\text{Threshold}}=2.370\times10^3$ s/mm^2, and the CNR values were 4.1 and 9.2 for the DWI image at $b=1000$ s/mm^2 and $b_{\text{Threshold}}$, respectively. (**f**) Postoperative pathology results (hematoxylin and eosin, ×200). Tumor cells completely disrupted the muscularis propria and extended into the mesorectum, confirming staging as T3N2

Table 4 The diagnosis performance of ADC and $b_{\text{Threshold}}$ for the statistically significant prognostic factors

Prognostic factors	ADC			$b_{\text{Threshold}}$			Difference between areas (95% CI)	*p* value
	AUC (95% CI)	Sensitivity (%)	Specificity (%)	AUC (95% CI)	Sensitivity (%)	Specificity (%)		
Pathologic differentiation	0.868 (0.710–0.958)	100.0	69.0	0.810 (0.642–0.923)	100.0	55.2	0.057 (−0.066 to 0.181)	0.363
T stage	0.912 (0.766–0.981)	90.5	85.7	0.796 (0.626–0.913)	52.4	100.0	0.116 (−0.019 to 0.250)	0.092
N stage	/	/	/	0.735 (0.559–0.869)	85.70	66.70	/	/

ADC apparent diffusion coefficient, *AUC* area under the curve, *CI* confidence interval

that $b_{\text{Threshold}}$ maps may be used to distinguish T3-4 lesions from T1-2 lesions. Therefore, $b_{\text{Threshold}}$ maps could address the inconsistent ability of high-resolution MRI, the current standard of care, to accurately T-stage rectal cancer (i.e., the results for high-resolution MRI ranged from 44 to 100% per meta-analysis) [27, 28].

Our study showed no significant difference in ADC values between different N stages, while the mean $b_{\text{Threshold}}$ value in group N1-2 was significantly higher than that in group N0. Additionally, the ROC curve of the N stage showed a large AUC (> 0.7) for $b_{\text{Threshold}}$. Therefore, $b_{\text{Threshold}}$ might reflect the aggressiveness of tumor tissue more accurately. This finding is especially promising because effective treatment depends on the accurate diagnosis of lymph node metastases, but the prediction of N staging in rectal cancer remains difficult [29], with reported accuracies of routine MRI-based lymph node staging ranging from 43 to 85% [30].

The analysis results from perineural invasion, LVI, tumor deposits, and tumor marker-based subgroups using both the ADC and $b_{\text{Threshold}}$ values failed to demonstrate a significant difference, findings that are partially consistent with the results of a study by Tang et al. [31]. These results may be

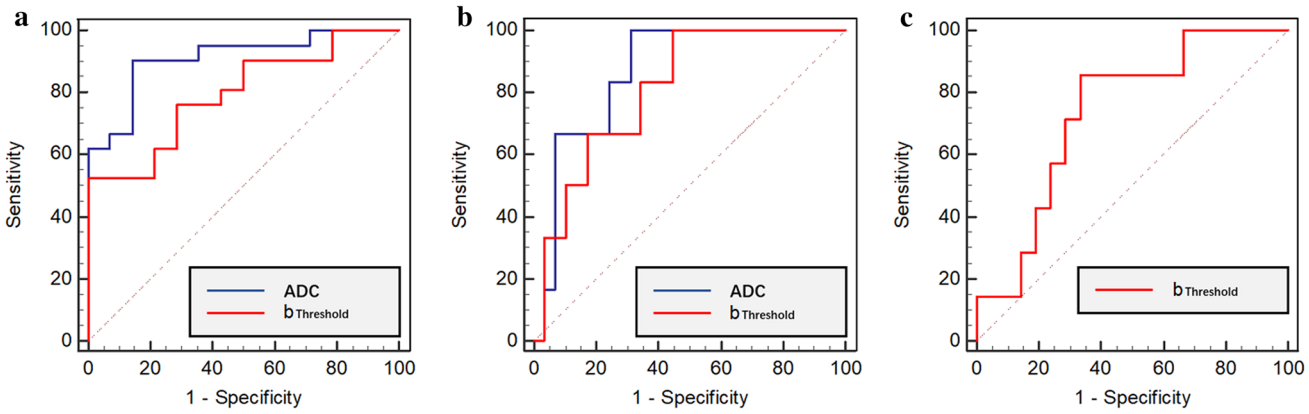

Fig. 4 Receiver operating characteristic (ROC) curves of the mean ADC and $b_{Threshold}$ values for the statistically significant prognostic factors. ROC plots for differentiating pathologic differentiation (**a**), T (**b**) and N stages (**c**) using ADC and $b_{Threshold}$ values. Areas under receiver operating characteristic curves are 0.868 and 0.912 for discriminating between differentiation and T stage using the ADC values, respectively. The areas under the receiver operating characteristic curves were 0.810, 0.796, and 0.735 for discriminating between differentiation, T and N stages using the $b_{Threshold}$ values, respectively. However, no significant differences were observed between the areas for pathologic differentiation (0.057, $p=0.363$) and T stage (0.116, $p=0.092$)

related to the study's small sample size or lack of special characteristics of these factors.

There were several limitations in this study. First, the sample size was relatively small. Large prospective multicenter trials are necessary to fully evaluate the role of the $b_{Threshold}$ map in assessing the pathological features of rectal cancer. Second, we only evaluated rectal adenocarcinomas without distant metastases; other types of rectal lesions were not included in the present study. Third, an experienced threshold of 50 (a.u.) for $b_{Threshold}$ was used in the current study and it may not be the best optimized one. Finally, this was a retrospective study that may be prone to selection bias. Further studies with more patients and more lesion types should be conducted to validate the present study's current results for rectal cancer diagnosis.

Conclusion

In conclusion, compared with DWI, the $b_{Threshold}$ map offers significantly higher CNR, which improves lesion visualization and detection. $b_{Threshold}$ values could differentiate between pathologic differentiation degrees and T stages and have a better diagnostic performance than ADC for N staging. Thus, the $b_{Threshold}$ map may serve as an assistant to DWI and ADC to evaluate the pathological features of rectal adenocarcinoma.

Acknowledgements This work was supported by the National Key Clinical Specialist Construction Programs of China and the Youth Initiative Fund of Second Military Medical University (Grant No. 2018QN05).

Author contributions CF and XY are employees of Siemens Healthcare (Shenzhen and Shanghai, China, respectively). FS, LC, and JL who are not employees of Siemens Healthcare had control of the data and information submitted for publication.

Compliance with ethical standards

Conflict of interest The authors declare that they have no conflict of interest.

References

1. Bray F, Ferlay J, Soerjomataram I, Siegel RL, Torre LA, Jemal A (2018) Global cancer statistics 2018: GLOBOCAN estimates of incidence and mortality worldwide for 36 cancers in 185 countries. CA Cancer J Clin 68 (6):394-424. https://doi.org/10.3322/caac.21492
2. Pan R, Zhu M, Yu C, Lv J, Guo Y, Bian Z, Yang L, Chen Y, Hu Z, Chen Z, Li L, Shen H, China Kadoorie Biobank Collaborative G (2017) Cancer incidence and mortality: A cohort study in China, 2008-2013. Int J Cancer 141 (7):1315-1323. https://doi.org/10.1002/ijc.30825
3. Benson AB, Venook AP, Al-Hawary MM, Cederquist L, Chen Y-J, Ciombor KK, Cohen S, Cooper HS, Deming D, Engstrom PF, Grem JL, Grothey A, Hochster HS, Hoffe S, Hunt S, Kamel A, Kirilcuk N, Krishnamurthi S, Messersmith WA, Meyerhardt J, Mulcahy MF, Murphy JD, Nurkin S, Saltz L, Sharma S, Shibata D, Skibber JM, Sofocleous CT, Stoffel EM, Stotsky-Himelfarb E, Willett CG, Wuthrick E, Gregory KM, Gurski L, Freedman-Cass DA (2018) Rectal Cancer, Version 2.2018, NCCN Clinical Practice Guidelines in Oncology. Journal of the National

Comprehensive Cancer Network 16 (7):874-901. https://doi.org/10.6004/jnccn.2018.0061
4. Lee YC, Hsieh CC, Chuang JP (2013) Prognostic significance of partial tumor regression after preoperative chemoradiotherapy for rectal cancer: a meta-analysis. Dis Colon Rectum 56(9):1093-1101. https://doi.org/10.1097/DCR.0b013e318298e36b
5. Lambregts DMJ, van Heeswijk MM, Delli Pizzi A, van Elderen SGC, Andrade L, Peters N, Kint PAM, Osinga-de Jong M, Bipat S, Ooms R, Lahaye MJ, Maas M, Beets GL, Bakers FCH, Beets-Tan RGH (2017) Diffusion-weighted MRI to assess response to chemoradiotherapy in rectal cancer: main interpretation pitfalls and their use for teaching. Eur Radiol 27 (10):4445-4454. https://doi.org/10.1007/s00330-017-4830-z
6. Bassaneze T, Goncalves JE, Faria JF, Palma RT, Waisberg J (2017) Quantitative Aspects of Diffusion-weighted Magnetic Resonance Imaging in Rectal Cancer Response to Neoadjuvant Therapy. Radiol Oncol 51 (3):270-276. https://doi.org/10.1515/raon-2017-0025
7. Iannicelli E, Di Pietropaolo M, Pilozzi E, Osti MF, Valentino M, Masoni L, Ferri M (2016) Value of diffusion-weighted MRI and apparent diffusion coefficient measurements for predicting the response of locally advanced rectal cancer to neoadjuvant chemoradiotherapy. Abdom Radiol (NY) 41 (10):1906-1917. https://doi.org/10.1007/s00261-016-0805-9
8. Koh DM, Collins DJ (2007) Diffusion-weighted MRI in the body: applications and challenges in oncology. AJR Am J Roentgenol 188 (6):1622-1635. https://doi.org/10.2214/AJR.06.1403
9. Sun Y, Tong T, Cai S, Bi R, Xin C, Gu Y (2014) Apparent Diffusion Coefficient (ADC) value: a potential imaging biomarker that reflects the biological features of rectal cancer. PLoS One 9 (10):e109371. https://doi.org/10.1371/journal.pone.0109371
10. Hausmann D, Liu J, Budjan J, Reichert M, Ong M, Meyer M, Smakic A, Grimm R, Strecker R, Schoenberg SO, Wang X, Attenberger UI (2018) Image Quality Assessment of 2D versus 3D T2WI and Evaluation of Ultra-high b-Value (b=2,000 mm/s(2)) DWI for Response Assessment in Rectal Cancer. Anticancer Res 38 (2):969-978. https://doi.org/10.21873/anticanres.12311
11. Delli Pizzi A, Caposiena D, Mastrodicasa D, Trebeschi S, Lambregts D, Rosa C, Cianci R, Seccia B, Sessa B, Di Flamminio FM, Chiacchiaretta P, Caravatta L, Cinalli S, Di Sebastiano P, Caulo M, Genovesi D, Beets-Tan R, Basilico R (2019) Tumor detectability and conspicuity comparison of standard b1000 and ultrahigh b2000 diffusion-weighted imaging in rectal cancer. Abdom Radiol (NY). https://doi.org/10.1007/s00261-019-02177-y
12. Porter DA, Heidemann RM (2009) High resolution diffusion-weighted imaging using readout-segmented echo-planar imaging, parallel imaging and a two-dimensional navigator-based reacquisition. Magn Reson Med 62 (2):468-475. https://doi.org/10.1002/mrm.22024
13. Feng Q, Yan YQ, Zhu J, Xu JR (2014) T staging of rectal cancer: accuracy of diffusion-weighted imaging compared with T2-weighted imaging on 3.0 tesla MRI. J Dig Dis 15 (4):188-194. https://doi.org/10.1111/1751-2980.12124
14. Heijnen LA, Lambregts DM, Mondal D, Martens MH, Riedl RG, Beets GL, Beets-Tan RG (2013) Diffusion-weighted MR imaging in primary rectal cancer staging demonstrates but does not characterise lymph nodes. Eur Radiol 23 (12):3354-3360. https://doi.org/10.1007/s00330-013-2952-5
15. Intven M, Reerink O, Philippens ME (2014) Repeatability of diffusion-weighted imaging in rectal cancer. J Magn Reson Imaging 40 (1):146-150. https://doi.org/10.1002/jmri.24337
16. Jung SH, Heo SH, Kim JW, Jeong YY, Shin SS, Soung MG, Kim HR, Kang HK (2012) Predicting response to neoadjuvant chemoradiation therapy in locally advanced rectal cancer: diffusion-weighted 3 Tesla MR imaging. J Magn Reson Imaging 35 (1):110-116. https://doi.org/10.1002/jmri.22749
17. Nougaret S, Reinhold C, Mikhael HW, Rouanet P, Bibeau F, Brown G (2013) The use of MR imaging in treatment planning for patients with rectal carcinoma: have you checked the "DISTANCE"? Radiology 268 (2):330-344. https://doi.org/10.1148/radiol.13121361
18. Pham TT, Liney G, Wong K, Rai R, Lee M, Moses D, Henderson C, Lin M, Shin JS, Barton MB (2017) Study protocol: multiparametric magnetic resonance imaging for therapeutic response prediction in rectal cancer. BMC Cancer 17 (1):465. https://doi.org/10.1186/s12885-017-3449-4
19. Gall P, Kasibhatla R, Meyer H (2014) Improved lesion visualization using b-value maps based on thresholded DWI images. Paper presented at the ISMRM, #6639
20. Chen L, Shen F, Li Z, Lu H, Chen Y, Wang Z, Lu J (2018) Diffusion-weighted imaging of rectal cancer on repeatability and cancer characterization: an effect of b-value distribution study. Cancer Imaging 18(1):43. https://doi.org/10.1186/s40644-018-0177-1
21. Sun Y, Hu P, Wang J, Shen L, Xia F, Qing G, Hu W, Zhang Z, Xin C, Peng W, Tong T, Gu Y (2018) Radiomic features of pretreatment MRI could identify T stage in patients with rectal cancer: Preliminary findings. J Magn Reson Imaging. https://doi.org/10.1002/jmri.25969
22. Edge SB, Byrd DR, Compton CC, Fritz AG, Greene FL, Trotti A, editors (2010) AJCC cancer staging manual. 7th edn. Springer, New York, NY
23. Shrout PE, Fleiss JL (1979) Intraclass correlations: uses in assessing rater reliability. Psychol Bull 86(2):420–428. https://doi.org/10.1037//0033-2909.86.2.420
24. Akashi M, Nakahusa Y, Yakabe T, Egashira Y, Koga Y, Sumi K, Noshiro H, Irie H, Tokunaga O, Miyazaki K (2014) Assessment of aggressiveness of rectal cancer using 3-T MRI: correlation between the apparent diffusion coefficient as a potential imaging biomarker and histologic prognostic factors. Acta Radiol 55 (5):524-531. https://doi.org/10.1177/0284185113503154
25. Cho EY, Kim SH, Yoon JH, Lee Y, Lim YJ, Kim SJ, Baek HJ, Eun CK (2013) Apparent diffusion coefficient for discriminating metastatic from non-metastatic lymph nodes in primary rectal cancer. Eur J Radiol 82 (11):e662-668. https://doi.org/10.1016/j.ejrad.2013.08.007
26. Curvo-Semedo L, Lambregts DM, Maas M, Beets GL, Caseiro-Alves F, Beets-Tan RG (2012) Diffusion-weighted MRI in rectal cancer: apparent diffusion coefficient as a potential noninvasive marker of tumor aggressiveness. J Magn Reson Imaging 35 (6):1365-1371. https://doi.org/10.1002/jmri.23589
27. Al-Sukhni E, Milot L, Fruitman M, Beyene J, Victor JC, Schmocker S, Brown G, McLeod R, Kennedy E (2012) Diagnostic accuracy of MRI for assessment of T category, lymph node metastases, and circumferential resection margin involvement in patients with rectal cancer: a systematic review and meta-analysis. Ann Surg Oncol 19 (7):2212-2223. https://doi.org/10.1245/s10434-011-2210-5
28. Dewhurst C, Rosen MP, Blake MA, Baker ME, Cash BD, Fidler JL, Greene FL, Hindman NM, Jones B, Katz DS, Lalani T, Miller FH, Small WC, Sudakoff GS, Tulchinsky M, Yaghmai V, Yee J (2012) ACR Appropriateness Criteria pretreatment staging of colorectal cancer. J Am Coll Radiol 9 (11):775-781. https://doi.org/10.1016/j.jacr.2012.07.025
29. Tezcan D, Turkvatan A, Turkoglu MA, Bostanci EB, Sakaogulllari Z (2013) Preoperative staging of colorectal cancer: accuracy of single portal venous phase multidetector computed tomography.

Clin Imaging 37 (6):1048-1053. https://doi.org/10.1016/j.clinimag.2013.08.003
30. Bipat S, Glas AS, Slors FJ, Zwinderman AH, Bossuyt PM, Stoker J (2004) Rectal cancer: local staging and assessment of lymph node involvement with endoluminal US, CT, and MR imaging--a meta-analysis. Radiology 232 (3):773-783. https://doi.org/10.1148/radiol.2323031368
31. Tang C, Lin MB, Xu JL, Zhang LH, Zuo XM, Zhang ZS, Liu MX, Xu JM (2018) Are ADC values of readout-segmented echo-planar diffusion-weighted imaging (RESOLVE) correlated with pathological prognostic factors in rectal adenocarcinoma? World J Surg Oncol 16 (1):138. https://doi.org/10.1186/s12957-018-1445-z